doi:10.1093/brain/awy307 BRAIN 2019: 142; 23–34 | 23

BRAIN
A JOURNAL OF NEUROLOGY

High prevalence of KRAS/BRAF somatic mutations in brain and spinal cord arteriovenous malformations

Tao Hong,[1,*] Yupeng Yan,[2,*] Jingwei Li,[1,*] Ivan Radovanovic,[3] Xiangyuan Ma,[4] Yang W. Shao,[4,5] Jiaxing Yu,[1] Yongjie Ma,[1] Peng Zhang,[1] Feng Ling,[1] Shuchen Huang,[2] Hongqi Zhang[1] and Yibo Wang[2]

*These authors contributed equally to this work.

Brain and spinal arteriovenous malformations are congenital lesions causing intracranial haemorrhage or permanent disability especially in young people. We investigated whether the vast majority or all brain and spinal arteriovenous malformations are associated with detectable tumour-related somatic mutations. In a cohort of 31 patients (21 with brain and 10 with spinal arteriovenous malformations), tissue and paired blood samples were analysed with ultradeep next generation sequencing of a panel of 422 common tumour genes to identify the somatic mutations. We used droplet digital polymerase chain reaction to confirm the panel sequenced mutations and identify the additional low variant frequency mutations. The association of mutation variant frequencies and clinical features were analysed. The average sequencing depth was $1077 \pm 298\times$. High prevalence (87.1%) of *KRAS/BRAF* somatic mutations was found in brain and spinal arteriovenous malformations with no other replicated tumour-related mutations. The prevalence of *KRAS/BRAF* mutation was 81.0% (17 of 21) in brain and 100% (10 of 10) in spinal arteriovenous malformations. We detected activating *BRAF* mutations and two novel mutations in *KRAS* (p.G12A and p.S65_A66insDS) in CNS arteriovenous malformations for the first time. The mutation variant frequencies were negatively correlated with nidus volumes of brain ($P = 0.038$) and spinal ($P = 0.028$) arteriovenous malformations but not ages. Our findings support a causative role of somatic tumour-related mutations of *KRAS/BRAF* in the overwhelming majority of brain and spinal arteriovenous malformations. This pathway homogeneity and high prevalence implies the development of targeted therapies with RAS/RAF pathway inhibitors without the necessity of tissue genetic diagnosis.

1 Department of Neurosurgery, Xuanwu Hospital, Capital Medical University, Beijing, China
2 State Key Laboratory of Cardiovascular Disease, Fuwai Hospital, National Center for Cardiovascular Diseases, Chinese Academy of Medical Sciences and Peking Union Medical College, Beijing, China
3 Department of Neurosurgery, Toronto Western Hospital, University Health Network, Toronto, Canada
4 Translational Medicine Research Institute, Geneseeq Technology Inc., Toronto, Canada
5 Department of Public Health, Nanjing Medical University, Nanjing, China

Correspondence to: Yibo Wang, PhD
Fuwai Hospital, Chinese Academy of Medical Sciences and Peking Union Medical College
167 Beilishi Rd, Beijing, 100037, China
E-mail: yibowang@hotmail.com

Received July 1, 2018. Revised September 26, 2018. Accepted October 16, 2018. Advance Access publication December 12, 2018
© The Author(s) (2018). Published by Oxford University Press on behalf of the Guarantors of Brain. All rights reserved.
For permissions, please email: journals.permissions@oup.com

Downloaded from https://academic.oup.com/brain/article/142/1/23/5240918 by guest on 21 August 2022

Correspondence may also be addressed to: Hongqi Zhang, MD, PhD
Department of Neurosurgery, Xuanwu Hospital, Capital Medical University, 45 Changchun St, Beijing 100053, China
E-mail: xwzhanghq@163.com

Keywords: tumour-related somatic mutation; KRAS/BRAF; arteriovenous malformations

Abbreviations: BAVM = brain arteriovenous malformation; ddPCR = droplet digital polymerase chain reaction; NGS = next generation sequencing; SAVM = spinal arteriovenous malformation

Introduction

Arteriovenous malformations are fast-flow vascular malformations characterized by connections between feeding arteries and draining veins, and although rare, are 20 times more common in the CNS, including the brain and spinal cord (Gomes and Bernatz, 1970; Milton *et al.*, 2012). Brain arteriovenous malformations (BAVMs) occur in 1.3 per 100 000 patient years and are equally distributed across populations, while the prevalence of spinal arteriovenous malformations (SAVMs) is 1/10th of BAVMs and account for ~20–30% in all spinal vascular malformations (Cogen and Stein, 1983). Germline mutations can be associated with hereditary syndromes hallmarked by arteriovenous malformations, such as mutations in the TGF-β/SMAD pathway (Gallione *et al.*, 2004) in hereditary haemorrhagic telangectasia (HHT) or in the RAS p21 protein activator 1 (RASA1) in the capillary malformation-arteriovenous malformation syndrome (CM-AVM) (Eerola *et al.*, 2003; Lapinski *et al.*, 2018). However, sporadic vascular malformations are much more common and seem to be associated with somatic and not germline mutations. These include sporadic arteriovenous malformations, cavernous malformations (Couto *et al.*, 2017; Al-Olabi *et al.*, 2018; Nikolaev *et al.*, 2018), vascular anomalies found in Sturge-Weber syndrome (Shirley *et al.*, 2013; Nakashima *et al.*, 2014), lymphatic and venous malformations (Limaye *et al.*, 2009, 2015; Castel *et al.*, 2016; Castillo *et al.*, 2016) as well as vascular tumours such as haemangiomas. From these studies, the emerging picture is that most of these lesions are associated with mutations commonly found in cancer, mainly in the PI3K-AKT-mTOR in low vascular malformations including venous and lymphatic malformations (Karpathiou *et al.*, 2017) and RAS-MAPK pathway in high flow lesions including BAVMs (Al-Olabi *et al.*, 2018; Nikolaev *et al.*, 2018). Specifically, activating mutations in *KRAS*, such as p.G12V and p.G12D, which are major cancer drivers, are associated with BAVMs (Nikolaev *et al.*, 2018). However, only about 60% of BAVMs harboured *KRAS* mutations with a significant number of BAVMs remaining without detected mutations and no somatic mutations have been reported in SAVMs. Here, using ultradeep next generation sequencing (NGS) with a panel of 422 tumour genes, we investigated whether the vast majority or all BAVMs and SAVMs are associated with detectable tumour-related somatic mutations.

Materials and methods

Patient enrolment and sample preparation

Twenty-one BAVM patients and 10 SAVM patients who underwent surgical resection of the nidus at the Beijing Xuanwu Hospital in China were recruited to this study. The study was approved by the ethics committee of Beijing Xuanwu Hospital (NO.2016032) and written informed consents from all patients or their guardians was obtained before surgery. All of the arteriovenous malformation diagnoses were made with imaging and pathological examinations by the study team. Patients demonstrating sporadic unifocal BAVMs/SAVMs with defined nidus structure were included. Patients with family history of arteriovenous malformations or documented genetic vascular diseases were excluded.

After surgical resection, the nidus was dissected from the tissue and was cut into equal samples. Together with matched whole blood samples, one of the tissue samples was sent to the sequencing facility of Nanjing Geneseeq Biotechnology Inc. (Nanjing, China) for NGS and droplet digital polymerase chain reaction (ddPCR) analyses.

Sample processing and library preparation

Genomic DNA was extracted from tissue samples and matched whole blood samples using DNeasy® Blood and Tissue Kit (Qiagen) following the manufacturer's recommended protocols. For each sample, 1–2 μg genomic DNA was fragmented using the Covaris M220 sonication system (Covaris) to 300–350 bp. Fragmented DNA was processed through end-repairing, A-tailing, and adaptor ligation using KAPA Hyper Prep Kit (KAPA Biosystems, KK8504), followed by size selection and purification using Agencourt AMPure XP beads (Beckman Coulter) with an optimized manufacturer's protocol. Finally, libraries were amplified by PCR and purified using Agencourt AMPure XP beads. Sample quality control was performed using NanoDrop™ 2000 (Thermo Fisher Scientific) for A260/280 and A260/230 ratios, and Bioanalyzer 2100 with High Sensitivity DNA kit (Agilent Technologies, 5067-4627) for size distribution. Sample and library quantification was performed using Qubit 3.0 dsDNA HS Assays (Life Technology).

Target enrichment and NGS

For targeted sequencing, a customized biotinylated probe panel (Integrated DNA Technologies) covering the exonic regions of 422 solid tumour-related genes and the intronic regions of a

Downloaded from https://academic.oup.com/brain/article/142/1/23/5240918 by guest on 21 August 2022

selected subset of the genes was used for hybridization enrichment. Libraries with different sample indices were pooled together in desirable ratios for up to 2 µg of total library. Human Cot-1 DNA (Life Technologies) and xGen® Universal Blocking Oligos (Integrated DNA Technologies) were added as blocking reagents. Liquid-phase probe-based capture was performed with Dynabeads M-270 (Life Technologies) and xGen® Lockdown Hybridization and Wash Kit (Integrated DNA Technologies) according to the manufacturer's protocols. Captured libraries were on-beads PCR amplified with Illumina p5 (5′-AATGATACGGCGACCACCGA-3′) and p7 primers (5′-CAAGCAGAAGACGGCATACGAGAT-3′) by KAPA HiFi HotStart ReadyMix (KAPA biosystems), followed by purification using Agencourt AMPure XP beads.

Target-enriched libraries were quantified by qPCR using KAPA Library Quantification Kit (KAPA Biosystems). Sequencing was carried out on HiSeq4000 NGS platforms (Illumina) according to the manufacturer's instructions, with paired-end 150 bp sequencing chemistry. Sequencing depth was anticipated to be 1000× and 100× for tissue sample and whole blood samples, respectively.

Sequencing data analysis

Sample demultiplexing was carried out using bcl2fastq v2.16.0.10 (Illumina). Adaptor nucleotides and low quality base cells were removed by Trimmomatics (Bolger *et al.*, 2014). Paired-end sequencing reads were aligned to the human reference genome hg19 (Genome Reference Consortium Human Reference 37, GRCh37) using Burrows-Wheeler Aligner v0.7.12 (BWA-MEM) (Li and Durbin, 2009). Samtools v1.6 was used to sort and index the aligned bam file (Li *et al.*, 2009). The bam file was further processed for PCR-duplicate removal by Picard v1.119 (https://broadinstitute.github.io/picard/) and for base recalibration and indel realignment by the Genome Analysis Toolkit v3.6 (GATK) (McKenna *et al.*, 2010).

MuTect somatic mode with default parameters was used for single nucleotide variant (SNV) identification (Cibulskis *et al.*, 2013). SNV displaying >1% population frequency within the 1000 Genomes project and dbSNP were also excluded (Sherry *et al.*, 2001; Genomes Project *et al.*, 2015). Small insertions and deletions (indels) were detected using Scalpel (Fang *et al.*, 2016). Identified SNVs and indels were annotated with ANNOVAR (Wang *et al.*, 2010), and manually reviewed on Integrative Genomics Viewer (IGV).

Droplet digital polymerase chain reaction

To validate the NGS results, and to screen additional low variant frequency mutations that were below the detection limit of NGS method, ddPCR was carried out on all of our samples.

Detection of rare variants in *KRAS* (NM_004985.3) and *BRAF* (NM_004333.4) was performed on the QX200 ddPCR system (Bio-Rad). Primers and probes for *KRAS* c.191_196 dupACAGTG p.Ser65_Ala66insAspSer were customized and synthesized at Integrated DNA Technologies (IDT) with the following sequences: forward primer 5′-TGGAGAAACCTGTCT CTTGGA-3′, reverse primer 5′-CCCTCCCCAGTCCTCATG TA-3′, reference allele locked nucleic acid (LNA) probe 5′-FAM-TCTCGACACAGCA-3′, insertion allele specific LNA probe 5′-HEX-ACAGTGACAGTGCA-3′. Each reaction was set up containing 50 ng genomic DNA, 9 pmol of each primer, 5 pmol of each probe, and 10 µl of 2× ddPCR Supermix for probes (No dUTP) (Bio-Rad) in a 20 µl reaction volume. The following PCR conditions were used: (i) an initial activation step at 95°C for 10 min; (ii) followed by 45 cycles of denaturation at 94°C for 30 s and annealing/elongation at 60°C for 1 min; (iii) followed by a final elongation at 60°C for 5 min. PCR temperature ramp rate was set at 2°C/s for every step. Primers and probes for *KRAS* c.35G>A p.Gly12Asp (dHsaMDV2510596), *KRAS* c.35G>T p.Gly12Val (dHsaMDV2510592), *KRAS* c.35G>C p.Gly12Ala (dHsaMDV2510586), *KRAS* c.183A>T p.Gln61His (dHsaMDV2010131), *KRAS* c.181C>A p.Gln61Lys (dHsaMDV2511862), *KRAS* c.34G>T p.Gly12Cys (dHsaMDV2510584), and *BRAF* c.1799T>A p.Val600Glu (dHsaCP2000027 and dHsaCP2000028) were purchased from Bio-Rad. Each reaction was set up following the manufacturer's instructions and containing 50 ng genomic DNA. PCR was carried out following the manufacturer's instructions for each commercial assay. PCR products were then subjected to analysis by the QX-200 droplet reader and QuantaSoft™ Analysis Software (Bio-Rad). A sample is considered positive if it displays at least three positive droplets, and if the number of positive droplets is at least three times the average number of positive droplets observed in five replicates of NA18535 negative control. The concentrations of target alleles were calculated using QuantaSoft™ version 1.7.4 (Bio-Rad) based on Poisson distribution.

Statistical analysis

Student's *t*-test and Pearson correlation were used to assess the difference and correlation between two groups of quantitative variables. A two-tailed probability value of 0.05 or less was considered statistically significant. Additional information can be found in the Supplementary material.

Data availability

The authors are willing to provide the raw data related to this manuscript upon request.

Results

Clinicopathological characteristics of patients

This cohort consisted of 22 males (71.0%) and nine (29.0%) females with a mean age of 28.6 ± 14.0 years (range 5–54 years). All patients had fresh nidus samples and matched blood samples. Twenty cases (64.5%) had ruptured BAVMs or SAVMs. Of the 21 patients with BAVMs, five had a Spetzler-Martin (SM) grade I, six a SM grade II, nine a SM grade III and one a SM grade IV lesion. Of the 10 patients with SAVMs, four had a type II (glomus) and six a type III (juvenile) SAVM (Table 1 and Fig. 1).

Downloaded from https://academic.oup.com/brain/article/142/1/23/5240918 by guest on 21 August 2022

Table 1 Study participants, tissue samples and study overview

Patient	Type	Age	Gender	Rupture	Location	Size, mm	High risk structure[a]	Deep venous drainage	Spetzler-Martin grades (BAVM)	Glomus/juvenile type (SAVM)
1	SAVM	34	M	Y	Cervical spinal cord (C5)	20.31 × 12.38 × 10.07	Y	-	-	Glomus
2	BAVM	28	M	N	Right frontal lobe of brain	23.69 × 19.46 × 17.86	N	N	I	-
3	BAVM	17	M	Y	Right parietal lobe of brain	45.99 × 37.01 × 29.93	N	N	III	-
4	BAVM	54	F	Y	Right frontal lobe of brain	32.35 × 29.71 × 28.02	N	N	I	-
5	BAVM	44	M	N	Right temporal lobe of brain	25.38 × 25.36 × 17.68	N	N	I	-
6	SAVM	21	F	N	Thoracic spinal cord (T12)	20.08 × 10.89 × 8.63	Y	-	-	Glomus
7	BAVM	48	M	Y	Left cerebellum	44.18 × 34.71 × 27.00	Y	Y	III	-
8	SAVM	45	F	Y	Cervical spinal cord (C7)	22.21 × 9.31 × 10.43	Y	-	-	Juvenile
9	SAVM	45	M	N	Thoracic spinal cord (T6)	13.17 × 7.78 × 9.01	N	-	-	Juvenile
10	SAVM	25	M	Y	Cervical spinal cord (C3)	16.99 × 11.75 × 10.19	N	-	-	Glomus
11	BAVM	10	M	Y	Left parietal lobe of brain	27.32 × 22.80 × 19.49	Y	Y	III	-
12	BAVM	36	F	Y	Left cerebellum	25.01 × 20.02 × 13.08	N	N	I	-
13	BAVM	52	M	Y	Left occipital lobe of brain	37.49 × 36.33 × 21.12	N	N	II	-
14	BAVM	29	F	N	Left frontal lobe of brain	40.81 × 30.16 × 27.90	N	N	II	-
15	BAVM	31	M	N	Right temporal lobe of brain	44.05 × 41.32 × 33.37	Y	N	IV	-
16	BAVM	11	M	Y	Left temporal lobe of brain	38.31 × 25.83 × 19.00	Y	Y	II	-
17	BAVM	13	M	Y	Right occipital lobe of brain	37.21 × 29.57 × 29.52	Y	N	III	-
18	BAVM	5	M	N	Left occipital lobe of brain	27.56 × 22.26 × 18.45	N	Y	I	-
19	BAVM	15	M	Y	Right cerebellum	40.01 × 28.16 × 24.60	Y	N	III	-
20	BAVM	43	F	Y	Right parietal lobe of brain	38.63 × 38.41 × 24.13	Y	N	III	-
21	SAVM	28	M	Y	Cervical spinal cord (C2)	13.54 × 9.90 × 6.89	N	-	-	Juvenile
22	SAVM	28	M	N	Thoracic spinal cord (T12)	24.21 × 12.21 × 8.09	Y	-	-	Juvenile
23	SAVM	16	M	N	Thoracic spinal cord (T7)	7.37 × 4.32 × 4.02	N	-	-	Juvenile
24	BAVM	48	M	Y	Left parietal lobe of brain	32.58 × 31.45 × 31.45	Y	N	III	-
25	BAVM	11	F	Y	Right parietal lobe of brain	NA[b]	N	N	II	-
26	BAVM	43	M	N	Left temporal lobe of brain	40.71 × 25.34 × 40.31	Y	N	II	-
27	SAVM	14	M	Y	Thoracic spinal cord (T12)	20.38 × 9.90 × 9.26	Y	-	-	Juvenile
28	BAVM	22	F	Y	Left temporal lobe of brain	33.91 × 28.40 × 15.45	Y	Y	III	-
29	SAVM	11	M	Y	Cervical spinal cord (C4–5)	14.77 × 10.05 × 8.26	Y	-	-	Glomus
30	BAVM	42	F	Y	Right temporal lobe of brain	26.79 × 25.71 × 23.95	Y	Y	II	-
31	BAVM	18	M	N	Left parietal lobe of brain	49.61 × 49.45 × 46.23	N	N	III	-

[a]High risk structure includes aneurysm, pseudoaneurysm, venectasia and high-flow fistula.
[b]Nidus volume and largest diameter were not detected in Patient 25 due to emergency surgery.

Downloaded from https://academic.oup.com/brain/article/142/1/23/5240918 by guest on 21 August 2022

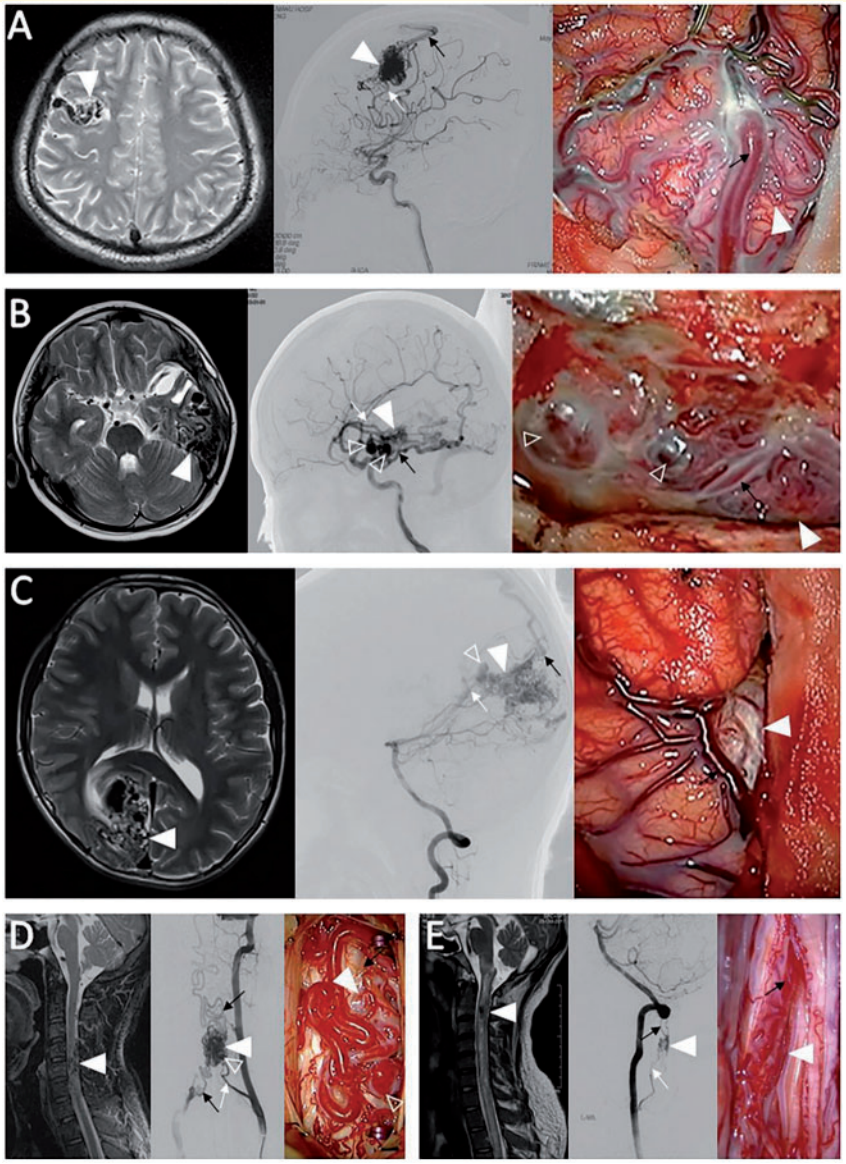

Figure 1 Representative MRI T_2-weighted, digital subtraction angiography (DSA) and intraoperative images of BAVMs/SAVMs included in this study. (**A**) Patient 2, right frontal lobe BAVM, *KRAS* p.G12D, ddPCR variant frequencies = 5.61%. (**B**) Patient 16, left temporal lobe BAVM, *BRAF* p.V600E, ddPCR variant frequencies = 2.99%. (**C**) Patient 17, occipital lobe BAVM, negative. (**D**) Patient 1, cervical SAVM, *KRAS* p.G12D, ddPCR variant frequencies = 4.40%. (**E**) Patient 21, cervical SAVM, *BRAF* p.V600E, ddPCR variant frequencies = 7.29%. Typical dark flow void signal on the MRI T_2-weighted images (*left*) indicate the niduses (white arrowhead) of arteriovenous malformation, which are surrounded by feeding arteries and draining veins. Feeding arteries (white arrow), nidus (white arrowhead), draining veins (black arrow) and high risk structure (white hollow arrowhead) can be identified clearly on the DSA (*middle*). Intraoperative images (*right*) demonstrate the tortuous dilated vessels on the surface of brain/spinal cord, of which the feeding arteries, nidus (white arrowhead), high risk structure (white hollow arrowhead), and the draining veins (black arrow) can be recognized easily.

Identification of somatic genetic variants by exome sequencing

Our panel included 422 tumour-related genes, the details of which can be found in Supplementary Table 1. As shown in Table 2, the average sequencing depth was $1077 \pm 298\times$. Among the 31 patients, 21 carried activating *KRAS* mutations and two carried *BRAF* mutations in tissue samples. None of patients were detected with corresponding mutations in paired blood samples. Except for mutations in genes of the RAS/RAF signalling pathway, no other gene mutations were found in nidus samples from more than two patients (Supplementary Table 1).

We found five single nucleotide missense variants and one insertion variant in the *KRAS* gene, with variant frequencies ranging from 0.13% to 8.82%. *KRAS* (NM_004985.3)

Downloaded from https://academic.oup.com/brain/article/142/1/23/5240918 by guest on 21 August 2022

Table 2 The results of NGS and ddPCR

Patient	Type	Tumour panel with 422 genes				ddPCR	
		Depth[a]	Mutant genes	*KRAS*/*BRAF* mutations	VF, %	*KRAS*/*BRAF* mutations[b]	VF, %
1	SAVM	1570.71	*KRAS*	*KRAS* c.35G>A	4.65	*KRAS* p.G12D	4.40
2	BAVM	1535.78	*KRAS*	*KRAS* c.35G>A	6.57	*KRAS* p.G12D	5.61
3	BAVM	1640.67	*KRAS*	*KRAS* c.35G>A	0.60	*KRAS* p.G12D	0.45
4	BAVM	1163.57	*KRAS*/*TET2*	*KRAS* c.35G>A	2.01	*KRAS* p.G12D	1.39
5	BAVM	775.55	*KRAS*	*KRAS* c.35G>A	2.50	*KRAS* p.G12D	2.95
6	SAVM	412.07	*KRAS*	*KRAS* c.35G>A	3.60	*KRAS* p.G12D	5.16
7	BAVM	1263.04	*KRAS*	*KRAS* c.35G>T	0.81	*KRAS* p.G12V	0.53
8	SAVM	1293.91	*KRAS*	*KRAS* c.35G>T	2.85	*KRAS* p.G12V	2.33
9	SAVM	443.22	*KRAS*	*KRAS* c.35G>T	8.82	*KRAS* p.G12V	7.10
10	SAVM	1187.50	*KRAS*	*KRAS* c.35G>C	4.86	*KRAS* p.G12A	4.85
11	BAVM	1469.84	*KRAS*	*KRAS* c.191_196dupACAGTG	5.56	*KRAS* p.S65_A66insDS	7.09
12	BAVM	1289.46	None	-	-	*KRAS* p.G12D	0.27
13	BAVM	1346.49	None	-	-	*KRAS* p.G12D	0.14
14	BAVM	1125.61	None	-	-	*KRAS* p.G12V	0.03
15	BAVM	1123.18	*KRAS*/*FLT4*	*KRAS* c.35G>A	1.52	*KRAS* p.G12D	1.47
16	BAVM	1296.57	*BRAF*/*KMT2C*	*BRAF* c.1799T>A	1.93	*BRAF* p.V600E	2.99
17	BAVM	1033.87	None	-	-	Negative	-
18	BAVM	1116.77	None	-	-	Negative	-
19	BAVM	994.44	*KRAS*/*CYP2D6*	*KRAS* c.35G>A	3.64	*KRAS* p.G12D	2.28
20	BAVM	978.54	None	-	-	*KRAS* p.G12V	1.20
21	SAVM	784.63	*BRAF*	*BRAF* c.1799T>A	6.54	*BRAF* p.V600E	7.29
22	SAVM	951.59	*KRAS*	*KRAS* c.183A>T	2.50	*KRAS* p.Q61H	2.22
23	SAVM	1269.42	*KRAS*	*KRAS* c.35G>A	5.58	*KRAS* p.G12D	5.72
24	BAVM	1154.37	*KRAS*/*DNMT3A*/*WAS*	*KRAS* c.35G>T	2.02	*KRAS* p.G12V	1.77
25	BAVM	898.58	*KRAS*	*KRAS* c.35G>A	0.72	*KRAS* p.G12D	0.44
26	BAVM	807.56	None	-	-	Negative	-
27	SAVM	1098.06	*KRAS*	*KRAS* c.34G>T	1.79	*KRAS* p.G12C	2.01
28	BAVM	946.65	*KRAS*/*FRG1*	*KRAS* c.35G>A	2.86	*KRAS* p.G12D	3.19
29	SAVM	950.56	*KRAS*	*KRAS* c.35G>T	7.23	*KRAS* p.G12V	7.13
30	BAVM	703.56	*KRAS*	*KRAS* c.35G>A	1.11	*KRAS* p.G12D	1.48
31	BAVM	776.58	None	-	-	Negative	-

[a]Average depth of the 422 tumour-related genes.
[b]Negative indicates that no positive mutations were found with *KRAS* p.G12A, p.G12D, p.G12V, p.Q61H, p.Q61K, p.A66delinsDSA, or *BRAF* p.V600E primers and probes.
VF = variant frequencies.

mutations were found at codon 12: c.35G>A p.Gly12Asp, c.35G>T p.Gly12Val, c.34G>T p.Gly12Cys, and c.35G>C p.Gly12Asp mutations; at codon 61 c.183A>T p.Gln61His mutation; and at codon 66 c.191_196dupACAGTG p.S65_Ala66insAspSer mutation. Activating mutation in *BRAF* (NM_004333.4) c.1799T>A p.Val600Glu was also observed in one SAVM patient and one BAVM patient. For simplicity, we use p.G12D, p.G12V, p.G12C, p.G12A, p.Q61H, p.S65_A66insDS, and p.V600E in this manuscript when referring to these mutations, respectively. Representative NGS results of these mutations were shown in Fig. 2. None of the seven mutations were annotated in the 1000 Genomes database. *KRAS* p.G12V, p.G12A and p.Q61H were not annotated in the ExAC Browser databases. *KRAS* p.G12D, p.G12C and *BRAF* p.V600E had ExAC allele counts of 2/101 204, 2/101 218 and 2/121 220, respectively. The other two mutations *KRAS* p.G12A, and p.S65_A66insDS have never previously been reported in SAVM and BAVM.

Confirmation of NGS mutations and identification of additional low variant frequency mutations with droplet digital PCR

The 21 *KRAS* and two *BRAF* mutations detected by panel sequencing of 422 panel genes were confirmed with ddPCR. Representative ddPCR results of these mutations are shown in Fig. 2. As shown in Table 2, four additional *KRAS* mutations were detected in eight exome sequencing-negative samples. The total prevalence of *KRAS*/*BRAF* mutations was therefore 87.1% (27 of 31) in our cohort. The variant frequencies of mutations verified by ddPCR ranged from 0.03% to 7.29%. The variant frequencies of the mutations determined by ddPCR showed strong correlation with the variant frequencies determined by NGS-based methods ($r = 0.950$, $P < 0.001$) (Supplementary Fig. 1).

Downloaded from https://academic.oup.com/brain/article/142/1/23/5240918 by guest on 21 August 2022

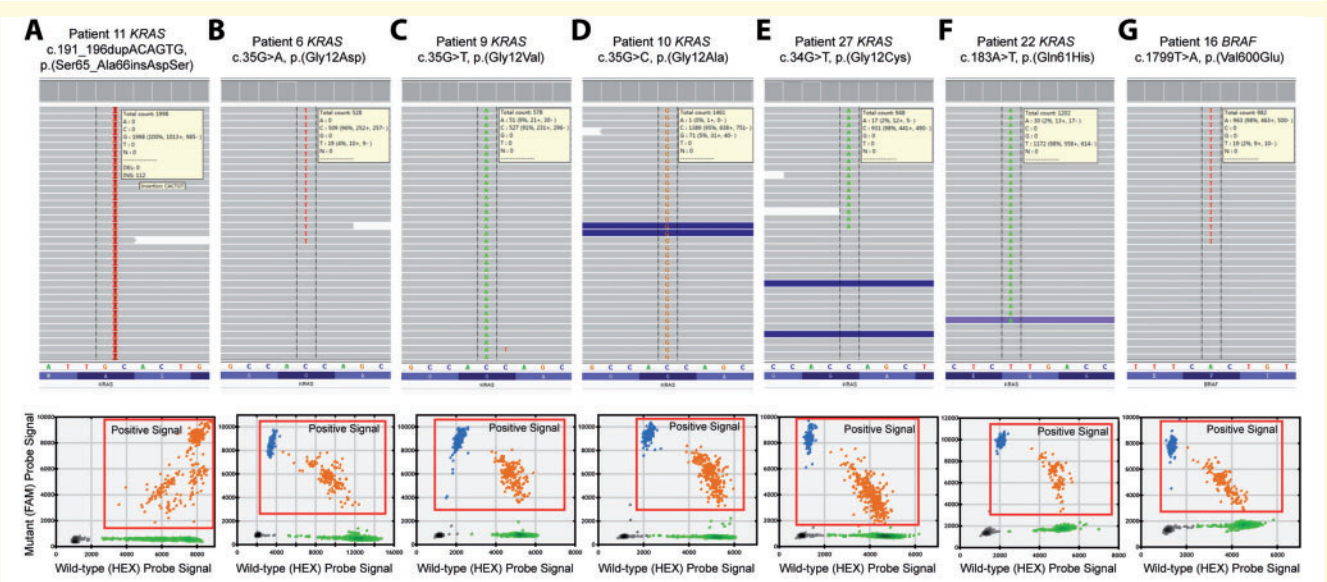

Figure 2 Representative Integrative Genomics Viewer snapshot of the NGS and ddPCR results of the seven *KRAS/BRAF* mutations identified in this study. *Top*: IGV snapshot. Each grey bar represents a sequencing read with base pairs matching the reference genome. Base cells deviating from the reference genome are considered as variants and are labelled. *Bottom*: 2D scatterplot of ddPCR results. Each dot represents a droplet. Blue: the droplet encloses at least one copy of mutant template. Green: the droplet encloses at least one copy of wild-type template. Orange: the droplet encloses at least one copy of wild-type and mutant template. Black: the droplet encloses no target molecular.

Spinal and brain arteriovenous malformations share mutations in *KRAS* and *BRAF*

The prevalence of *KRAS/BRAF* mutations was 81.0% (17 of 21) in BAVM and 100% (10 of 10) in SAVM. Both panel sequencing and ddPCR results showed that SAVMs and BAVMs shared the mutation pattern in *KRAS* and *BRAF*, with comparable prevalence. For example, *KRAS* p.G12D and p.G12V were mutation hotspots both in SAVMs and BAVMs, with a prevalence of 30.0% and 30.0% in SAVMs, and 52.4% and 19.0% in BAVMs, respectively, whereas *BRAF* p.V600E was rare and found in only one BAVM and one SAVM patient (Fig. 3).

Mutation variant frequencies are negatively correlated with nidus volumes and largest diameters, but not patient ages

Because of significant differences on nidus volume between SAVMs and BAVMs, we separately analysed their correlation with mutation variant frequencies in 10 patients with SAVM. The mutation variant frequency was negatively correlated with nidus volumes and largest diameters ($r = -0.686$, $P = 0.028$ in nidus volumes, and $r = -0.764$, $P = 0.010$ in nidus largest diameters, respectively). Similarly, in 20 patients with BAVM (nidus volume and largest diameter were not available in Patient 25 due to emergency surgery), the mutation variant frequencies were also negatively correlated with the two indices ($r = -0.522$, $P = 0.038$ in nidus volumes, and $r = -0.524$, $P = 0.037$ in nidus largest diameters, respectively). Furthermore, no significant correlation was found between mutation variant frequencies and ages ($r = -0.338$, $P = 0.085$) (Fig. 4). Furthermore, patients were divided into two groups with the same number of patients according to variant frequencies. Significant differences on nidus length and volume were observed between the two subgroups with low and high variant frequencies. As shown in Table 3, patients with low variant frequencies showed significantly larger lengths and volumes both in SAVM and in BAVM. In these analyses, we used ddPCR variant frequencies as the mutation variant frequencies.

Discussion

In this study, we profiled 31 CNS arteriovenous malformations, including BAVMs and SAVMs, for somatic mutations in a panel of 422 tumour-related genes. The key findings of our study are (i) high prevalence (nearly 90%) of *KRAS/BRAF* somatic mutations in BAVMs and SAVMs with no other tumour gene mutations replicated using ultradeep panel sequencing; (ii) the first evidence of activating *BRAF* mutations in BAVMs and SAVMs; and (iii) evidence that SAVMs, a disease previously uncharacterized at the genetic level, share the same highly prevalent mutations in *KRAS* and *BRAF* with BAVMs. Moreover, we also observed two novel mutations in *KRAS* (p.G12A and p.S65_A66insDS) in CNS arteriovenous malformations. Finally, we found that mutation variant frequencies negatively correlated with nidus volumes and largest diameters

Downloaded from https://academic.oup.com/brain/article/142/1/23/5240918 by guest on 21 August 2022

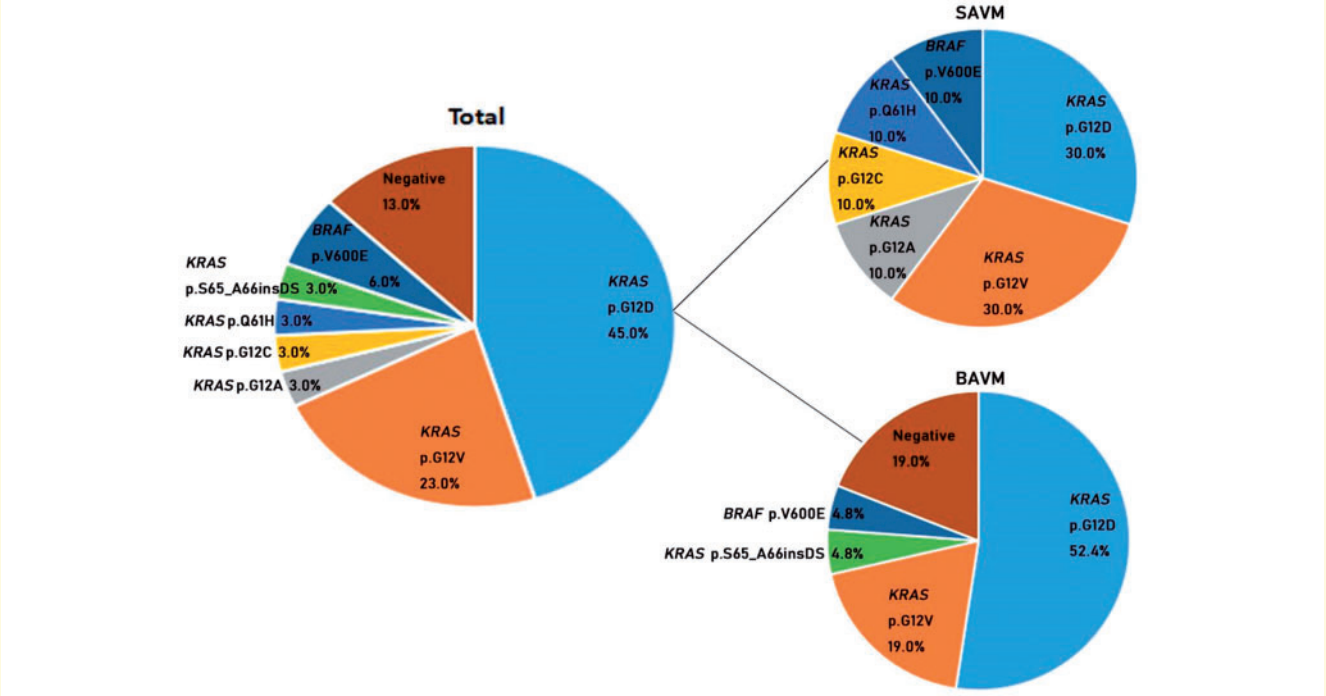

Figure 3 The prevalence of *KRAS/BRAF* mutations in SAVM and in BAVM.

but not with age, a finding that may have implications for the understanding of the pathogenesis of arteriovenous malformations.

High prevalence of somatic *KRAS/BRAF* mutation

Recently, activating somatic *KRAS* mutations were observed with a relatively high prevalence of 64% in BAVMs, and associated with the activation of the MAPK/ERK pathway, one of the major intracellular signalling pathway downstream of KRAS (Nikolaev *et al.*, 2018). Consistently, activated mosaic mutations in four MAPK pathway genes, i.e. *KRAS*, *NRAS*, *BRAF* and *MAP2K1* were described in intracranial and extracranial vascular malformations including high flow arteriovenous malformations (Couto *et al.*, 2017; Al-Olabi *et al.*, 2018), reinforcing the role of the RAS/RAF/MAPK/ERK pathway in arteriovenous malformations. Interestingly, BAVMs without detectable *KRAS* mutations also had high levels of phorphorylated ERK1/2, suggesting that the RAS/RAF/MAPK/ERK pathway activation is a hallmark of all BAVMs (Nikolaev *et al.*, 2018). Intriguingly, KRAS mutations as well as its downstream effector BRAF mutations also occurred at high frequency in endoderm-derived tumours and played a role in their progression, through the RAS-RAF-MEK-MAPK pathway or the PI3K-AKT-PTEN-mTOR pathway (shared the same upstreaming tyrosine kinase with RAS-RAF-MEK-MAPK) (Quinlan *et al.*, 2008; Millington, 2013; Simanshu *et al.*, 2017). Our study not only confirms the presence of activating *KRAS* mutations in BAVMs, but also finds a much higher prevalence of 87.1% of *KRAS/BRAF* mutation in BAVMs/SAVMs than previously reported values (Al-Olabi *et al.*, 2018; Nikolaev *et al.*, 2018). This difference is most likely accredited to the ultradeep sequencing (1077×) of a restricted panel of genes used in our study compared to the lower depth whole exome sequencing used by Nikolaev *et al.* (2018) and possibly differences in tissue preparation, ddPCR methodology and calling thresholds. Importantly, our study provides the first evidence of *BRAF* mutations in CNS arteriovenous malformations both in the brain and spinal cord. Knowing that a *BRAF* mutation has previously been found in only one arteriovenous malformation sample from an extracranial skin arteriovenous malformation (Al-Olabi *et al.*, 2018), which is again consistent with the centrality of the RAS/RAF/MAPK pathway in arteriovenous malformations.

The fact that all of the mutations found in arteriovenous malformations, including *KRAS* p.G12V and p.G12D, and *BRAF* p.V600E and *MAP2K1*, result in oncogenic activation of these genes and are all drivers of cancer growth in humans (Cichowski and Janne, 2010; Prior *et al.*, 2012; Simanshu *et al.*, 2017) contrasts with their presence in the majority of arteriovenous malformations, which are not tumoural vascular growths. This points to a tissue-specific and context-dependent role of the RAS/RAF/MAPK pathway in vascular tissue or perhaps a need for multiple additional genetic hits to sustain cancer as opposed to a monogenetic nature of arteriovenous malformations. This

Downloaded from https://academic.oup.com/brain/article/142/1/23/5240918 by guest on 21 August 2022

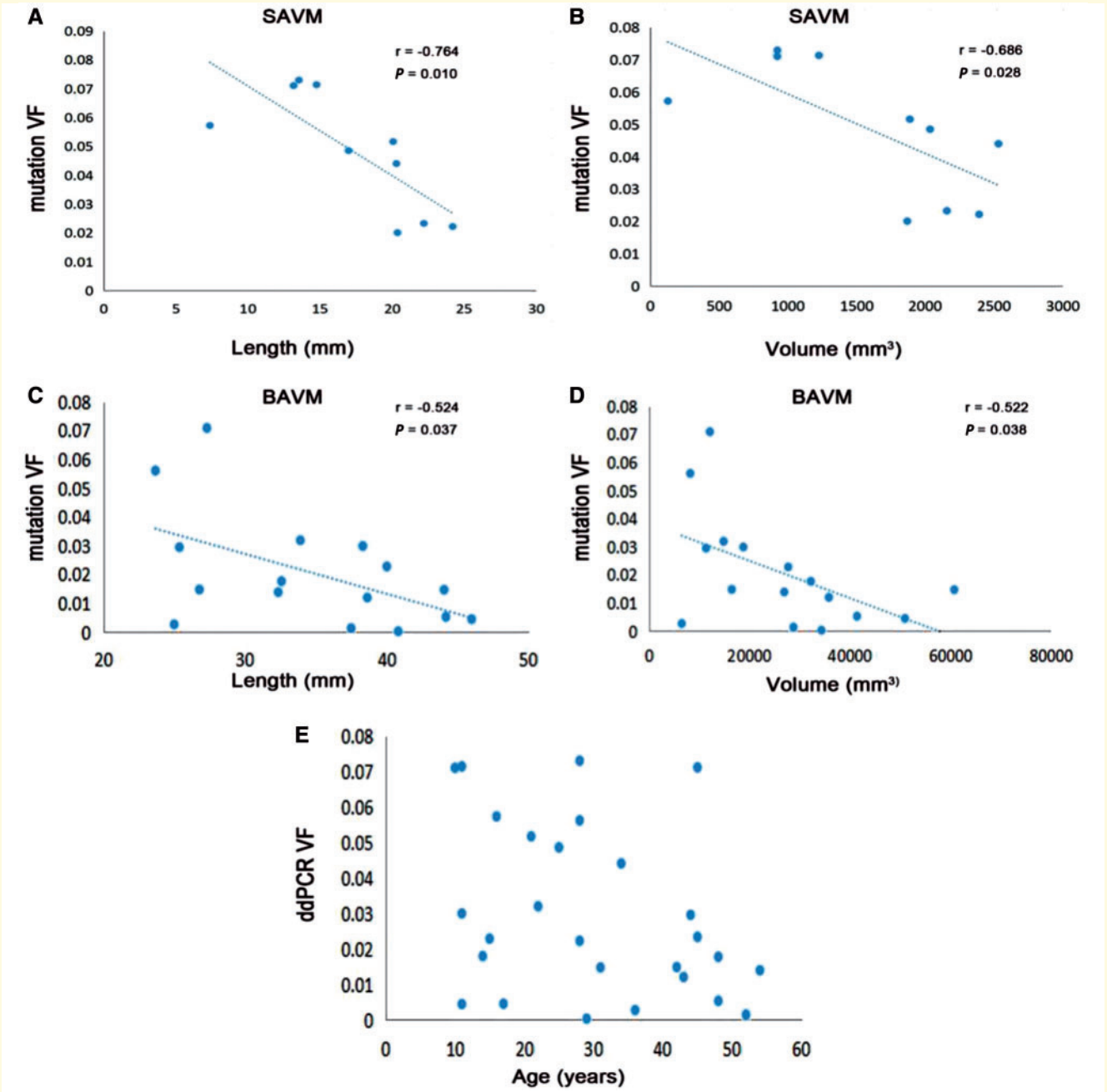

Figure 4 Mutation variant frequencies were negatively correlated with nidus volumes and largest diameters in both SAVMs and BAVMs, but not with patient age. (**A**) The mutation variant frequencies (VF) were negatively correlated with SAVM largest diameters, r = −0.764, *P* = 0.010. (**B**) The mutation variant frequencies were negatively correlated with SAVM nidus volumes, r = −0.686, *P* = 0.028. (**C**) The mutation variant frequencies were negatively correlated with BAVM largest diameters, r = −0.524, *P* = 0.037. (**D**) The mutation variant frequencies were negatively correlated with BAVM nidus volumes, r = −0.522, *P* = 0.038. (**E**) The mutation variant frequencies were not associated with patient ages, r = −0.338, *P* = 0.085.

Table 3 Significant difference on nidus length and volume between low and high variant frequency groups

	SAVM			BAVM		
	n	Length	Volume	*n*	Length	Volume
Low VF[a]	5	20.8 ± 2.7	2196.5 ± 267.5	8	38.6 ± 7.0	35 684.4 ± 16 337.7
High VF	5	13.8 ± 4.5	1017.6 ± 634.2	8	31.0 ± 6.1	17 733.9 ± 8301.3
P		0.017	0.005		0.038	0.015

[a]Patients were divided into two groups with the same number of patients according to variant frequencies (VF).

Downloaded from https://academic.oup.com/brain/article/142/1/23/5240918 by guest on 21 August 2022

monogenetic nature, most evident in our findings of *KRAS/BRAF* mutation in nearly 90% of BAVMs and SAVMs, renders inhibition of the RAS/RAF/MAPK/ERK with small molecule MEK inhibitors as an attractive option for future targeted therapies of BAVMs. BRAF and MEK inhibitors are already used in clinical practice for *BRAF* p.V600E mutated melanomas (Long *et al.*, 2014). Knowing that nearly all BAVMs and SAVMs have mutations in either *KRAS* or *BRAF*, permits the opportunity of initiating therapy in potential clinical trials without previous tissue sampling and genetic confirmation, which is not feasible in BAVMs or SAVMs outside of total resection.

Genetic homogeneity in SAVMs and BAVMs

BAVMs and SAVMs belong to CNS vascular malformations and may therefore share a similar pathogenesis, differing only by their different location along the neuraxis. Concomitant BAVM and SAVM patients have been reported in literature, which may be the evidence of the embryological homology (Hasegawa *et al.*, 1999; Wang *et al.*, 2009; Shallwani *et al.*, 2012). It may occur at a different site of neuraxis between the fourth and eighth weeks of embryonic development, then disperse and form the nidus in a different part of the CNS. Both, in addition to sharing angioarchitectural features of high flow arteriovenous malformations, are characterized by aberrant angiogenesis and vascular remodelling (Aminoff and Logue, 1974; Kim and Spetzler, 2006; Kawamoto and Losordo, 2008; Rangel-Castilla *et al.*, 2014). In our previous study, we demonstrated that both BAVMs and SAVMs share similar immunohistochemistry features (Gao *et al.*, 2010, 2011). Besides, endothelial cells, as well as the endothelial progenitor cells, mediate pathological vascular remodelling and impact the clinical course of both BAVM and SAVM. However, the genetic basis of SAVMs remains unexplored. Here, we elucidate the genetic basis of a majority of SAVMs, albeit in a small cohort of 10 patients, and show that they harbour the same somatic mutations in *BRAF* and *KRAS* with comparable prevalences as BAVMs. Our findings, together with previous studies on brain and extracranial arteriovenous malformations (Couto *et al.*, 2017; Al-Olabi *et al.*, 2018; Nikolaev *et al.*, 2018), may suggest a relative genetic homogeneity of all high flow arteriovenous malformations, within which mutations occur in different genes of the same signalling pathway.

KRAS/BRAF mutation variant frequency and arteriovenous malformation size

The finding of recurrent highly prevalent *KRAS/BRAF* mutations in both BAVMs and SAVMs, the pathogenic nature of those mutations, the absence of *KRAS/BRAF* mutations in brain vascular malformations other than BAVMs (Nikolaev *et al.*, 2018), and the direct induction of arteriovenous malformation-like lesions by a mutation in an animal model (Al-Olabi *et al.*, 2018), convergently support that *KRAS/BRAF* mutations are causative and not bystander events due to endothelial proliferation, angiogenic signalling or vascular remodelling in arteriovenous malformations. Moreover, the absence of correlation of mutation variant frequencies with patient age and the negative correlation with arteriovenous malformation size in our study, is inconsistent with a passenger mutation hypothesis where *KRAS/BRAF* mutations would randomly accumulate with time and lesion growth. On the contrary, a negative correlation between variant frequencies and arteriovenous malformation size may support the view that arteriovenous malformations result from the clonal progeny of an endothelial precursor acquiring a somatic mutation and initiating the pathogenesis of the arteriovenous malformations. In this scenario, with tissue growth and endothelial turnover, wild-type endothelial cells would also be incorporated in the arteriovenous malformation, therefore diluting the mutant arteriovenous malformation cells. However, the high cell heterogeneity of arteriovenous malformation tissue may be an alternative explanation of our findings. For example, a potentially different cell ratio between endothelial and mural cells in small and large arteriovenous malformations may also result in a dilution of mutation variant frequencies in large lesions. Further analysis of endothelial cells isolated from BAVMs and SAVMs would resolve this question.

Recently, *EPHB4* mutations were identified in vein of Galen aneurysmal malformation (Vivanti *et al.*, 2018), and somatic inactivating *RASA1* mutation was identified in capillary malformation lesion tissue in a patient with germline *RASA1* mutation (Lapinski *et al.*, 2018). Those genes involved in vascular malformation in previous studies could be potential somatic mutated genes in arteriovenous malformation tissues, such as *RASA1*, *EPHB4*, *ENG*, *ACVRL1*, *GDF2*, *NF1* etc. (Matsubara *et al.*, 2000; Eerola *et al.*, 2003; Mahmoud *et al.*, 2010; Chida *et al.*, 2013; Tualchalot *et al.*, 2014; Lapinski *et al.*, 2018; Vivanti *et al.*, 2018). Before targeted ultradeep 422-gene exome sequencing, whole exome sequencing was also performed in 12 of our cohort and no somatic mutations were detected within these genes. Despite that, we advocated the idea of profiling the genes whose hotspot mutations have been previously associated with vascular malformation when practicing clinical management of vascular malformation. A targeted exome NGS panel designated for arteriovenous malformations including both tumour-related somatic mutation genes and vascular malformation mutation genes should be developed in the future.

Another related unresolved question is whether *KRAS/BRAF* mutations are single and sufficient causative events in BAVMs and SAVMs or if another genetic event is required, either as a preceding germline or somatic mutation or an ulterior second hit. The injection of $BRAF^{V600E}$ into single-cell zebrafish embryos to generate post-zygotic

Downloaded from https://academic.oup.com/brain/article/142/1/23/5240918 by guest on 21 August 2022

expression, resulted in only 10–20% vascular malformation in a recent study (Al-Olabi *et al.*, 2018) and these authors speculated that the first hit is one germline mutation and/or other somatic mutation, and the second hit is *KRAS/BRAF* mutation, which eventually causes arteriovenous malformations. According to our results, we speculate that the *KRAS/BRAF* mutation is more likely the first hit. Future studies are needed to elucidate these mechanisms.

Conclusion

Our findings support a causative role of somatic activating mutations in *KRAS/BRAF* in the overwhelming majority of BAVMs and SAVMs. Practically and importantly, this pathway homogeneity in CNS arteriovenous malformations also supports the development of targeted therapies with RAS/RAF/MAPK pathway inhibitors without the necessity of tissue genetic diagnosis, a major obstacle if mutations were distinct pathways involved in arteriovenous malformations.

Acknowledgements

We want to thank all the patients at Beijing Xuanwu Hospital for their help on research coordination.

Funding

This study was supported by National Key R&D Program of China with grants 2016YFC1300800 to H.Z. and 2017YFC0909400 to Y.W.; National Natural Science Foundation of China with grants 81671202 to H.Z., 81701151 to T.H. and 81770424 to Y.W.; Beijing Municipal Science and Technology Commission with grant D161100003816001 to H.Z., D161100003816006 to T.H.; Beijing Municipal Administration of Hospitals' Ascent Plan with grant DFL20180801 to H.Z. and Chinese Academy of Medical Sciences with Innovation Fund for Medical Sciences CAMS2017-I2M-1-008 to Y.W.

Competing interests

X.M. and Y.W.S. are employees and/or shareholders of Geneseeq Technology Inc.

Supplementary material

Supplementary material is available at *Brain* online.

References

Al-Olabi L, Polubothu S, Dowsett K, Andrews KA, Stadnik P, Joseph AP, et al. Mosaic RAS/MAPK variants cause sporadic vascular malformations which respond to targeted therapy. J Clin Invest 2018; 128: 1496–508.

Aminoff MJ, Logue V. The prognosis of patients with spinal vascular malformations. Brain 1974; 97: 211–8.

Bolger AM, Lohse M, Usadel B. Trimmomatic: a flexible trimmer for Illumina sequence data. Bioinformatics 2014; 30: 2114–20.

Castel P, Carmona FJ, Grego-Bessa J, Berger MF, Viale A, Anderson KV, et al. Somatic PIK3CA mutations as a driver of sporadic venous malformations. Sci Transl Med 2016; 8: 332ra42.

Castillo SD, Tzouanacou E, Zaw-Thin M, Berenjeno IM, Parker VE, Chivite I, et al. Somatic activating mutations in Pik3ca cause sporadic venous malformations in mice and humans. Sci Transl Med 2016; 8: 332ra43.

Chida A, Shintani M, Wakamatsu H, Tsutsumi Y, Iizuka Y, Kawaguchi N, et al. ACVRL1 gene variant in a patient with vein of Galen aneurysmal malformation. J Pediatr Genet 2013; 02: 181–9.

Cibulskis K, Lawrence MS, Carter SL, Sivachenko A, Jaffe D, Sougnez C, et al. Sensitive detection of somatic point mutations in impure and heterogeneous cancer samples. Nat Biotechnol 2013; 31: 213–9.

Cichowski K, Janne PA. Drug discovery: inhibitors that activate. Nature 2010; 464: 358–9.

Cogen P, Stein BM. Spinal cord arteriovenous malformations with significant intramedullary components. J Neurosurg 1983; 59: 471–8.

Couto JA, Huang AY, Konczyk DJ, Goss JA, Fishman SJ, Mulliken JB, et al. Somatic MAP2K1 mutations are associated with extracranial arteriovenous malformation. Am J Hum Genet 2017; 100: 546–54.

Eerola I, Boon LM, Mulliken JB, Burrows PE, Dompmartin A, Watanabe S, et al. Capillary malformation-arteriovenous malformation, a new clinical and genetic disorder caused by RASA1 mutations. Am J Hum Genet 2003; 73: 1240–9.

Fang H, Bergmann EA, Arora K, Vacic V, Zody MC, Iossifov I, et al. Indel variant analysis of short-read sequencing data with Scalpel. Nat Protoc 2016; 11: 2529–48.

Gallione CJ, Repetto GM, Legius E, Rustgi AK, Schelley SL, Tejpar S, et al. A combined syndrome of juvenile polyposis and hereditary haemorrhagic telangiectasia associated with mutations in MADH4 (SMAD4). Lancet 2004; 363: 852–9.

Gao P, Chen Y, Lawton MT, Barbaro NM, Yang GY, Su H, et al. Evidence of endothelial progenitor cells in the human brain and spinal cord arteriovenous malformations. Neurosurgery 2010; 67: 1029–35.

Gao P, Zhang H, Ling F. Angiogenic and inflammatory factor expressions in cutaneomeningospinal angiomatosis (Cobb's syndrome): case report. Acta Neurochir (Wien) 2011; 153: 1657–61.

Genomes Project C, Auton A, Brooks LD, Durbin RM, Garrison EP, Kang HM, et al. A global reference for human genetic variation. Nature 2015; 526: 68–74.

Gomes MM, Bernatz PE. Arteriovenous fistulas: a review and ten-year experience at the Mayo Clinic. Mayo Clin Proc 1970; 45: 81–102.

Hasegawa S, Hamada JI, Morioka M, Kai Y, Takaki S, Ushio Y. Multiple cerebral arteriovenous malformations (AVMs) associated with spinal AVM. Acta Neurochir (Wien) 1999; 141: 315–9.

Karpathiou G, Chauleur C, Da Cruz V, Forest F, Peoc'h M. Vascular lesions of the female genital tract: clinicopathologic findings and application of the ISSVA classification. Pathophysiology 2017; 24: 161–7.

Kawamoto A, Losordo DW. Endothelial progenitor cells for cardiovascular regeneration. Trends Cardiovasc Med 2008; 18: 33–7.

Kim LJ, Spetzler RF. Classification and surgical management of spinal arteriovenous lesions: arteriovenous fistulae and arteriovenous malformations. Neurosurgery 2006; 59 (5 Suppl 3): S195–201; discussion S3–13.

Lapinski PE, Doosti A, Salato V, North P, Burrows PE, King PD. Somatic second hit mutation of RASA1 in vascular endothelial cells in capillary malformation-arteriovenous malformation. Eur J Med Genet 2018; 61: 11–16.

Downloaded from https://academic.oup.com/brain/article/142/1/23/5240918 by guest on 21 August 2022

Li H, Durbin R. Fast and accurate short read alignment with Burrows-Wheeler transform. Bioinformatics 2009; 25: 1754–60.
Li H, Handsaker B, Wysoker A, Fennell T, Ruan J, Homer N, et al. The sequence alignment/map format and SAMtools. Bioinformatics 2009; 25: 2078–9.
Limaye N, Kangas J, Mendola A, Godfraind C, Schlogel MJ, Helaers R, et al. Somatic activating PIK3CA mutations cause venous malformation. Am J Hum Genet 2015; 97: 914–21.
Limaye N, Wouters V, Uebelhoer M, Tuominen M, Wirkkala R, Mulliken JB, et al. Somatic mutations in angiopoietin receptor gene TEK cause solitary and multiple sporadic venous malformations. Nat Genet 2009; 41: 118–24.
Long GV, Stroyakovskiy D, Gogas H, Levchenko E, de Braud F, Larkin J, et al. Combined BRAF and MEK inhibition versus BRAF inhibition alone in melanoma. N Engl J Med 2014; 371: 1877–88.
Mahmoud M, Allinson KR, Zhai Z, Oakenfull R, Ghandi P, Adams RH, et al. Pathogenesis of arteriovenous malformations in the absence of endoglin. Circ Res 2010; 106: 1425–33.
Matsubara S, Bourdeau A, Terbrugge KG, Wallace C, Letarte M. Analysis of endoglin expression in normal brain tissue and in cerebral arteriovenous malformations. Stroke 2000; 31: 2653–60.
McKenna A, Hanna M, Banks E, Sivachenko A, Cibulskis K, Kernytsky A, et al. The genome analysis toolkit: a MapReduce framework for analyzing next-generation DNA sequencing data. Genome Res 2010; 20: 1297–303.
Millington GW. Mutations of the BRAF gene in human cancer, by Davies et al. (Nature 2002; 417: 949–54). Clin Exp Dermatol 2013; 38: 222–3.
Milton I, Ouyang D, Allen CJ, Yanasak NE, Gossage JR, Alleyne CH Jr, et al. Age-dependent lethality in novel transgenic mouse models of central nervous system arteriovenous malformations. Stroke 2012; 43: 1432–5.
Nakashima M, Miyajima M, Sugano H, Iimura Y, Kato M, Tsurusaki Y, et al. The somatic GNAQ mutation c.548G>A (p.R183Q) is consistently found in Sturge-Weber syndrome. J Hum Genet 2014; 59: 691–3.
Nikolaev SI, Vetiska S, Bonilla X, Boudreau E, Jauhiainen S, Rezai Jahromi B, et al. Somatic activating KRAS mutations in arteriovenous malformations of the brain. N Engl J Med 2018; 378: 250–61.
Prior IA, Lewis PD, Mattos C. A comprehensive survey of Ras mutations in cancer. Cancer Res 2012; 72: 2457–67.
Quinlan MP, Quatela SE, Philips MR, Settleman J. Activated Kras, but not Hras or Nras, may initiate tumors of endodermal origin via stem cell expansion. Mol Cell Biol 2008; 28: 2659–74.
Rangel-Castilla L, Russin JJ, Zaidi HA, Martinez-Del-Campo E, Park MS, Albuquerque FC, et al. Contemporary management of spinal AVFs and AVMs: lessons learned from 110 cases. Neurosurg Focus 2014; 37: E14.
Shallwani H, Tahir MZ, Bari ME, Tanveer Ul H. Concurrent intracranial and spinal arteriovenous malformations: report of two pediatric cases and literature review. Surg Neurol Int 2012; 3: 51.
Sherry ST, Ward MH, Kholodov M, Baker J, Phan L, Smigielski EM, et al. dbSNP: the NCBI database of genetic variation. Nucleic Acids Res 2001; 29: 308–11.
Shirley MD, Tang H, Gallione CJ, Baugher JD, Frelin LP, Cohen B, et al. Sturge-Weber syndrome and port-wine stains caused by somatic mutation in GNAQ. N Engl J Med 2013; 368: 1971–9.
Simanshu DK, Nissley DV, McCormick F. RAS proteins and their regulators in human disease. Cell 2017; 170: 17–33.
Tualchalot S, Mahmoud M, Allinson KR, Redgrave RE, Zhai Z, Oh SP, et al. Endothelial depletion of Acvrl1 in mice leads to arteriovenous malformations associated with reduced endoglin expression. PLoS One 2014; 9: e98646.
Vivanti A, Ozanne A, Grondin C, Saliou G, Quevarec L, Maurey H, et al. Loss of function mutations in EPHB4 are responsible for vein of Galen aneurysmal malformation. Brain 2018; 141: 979–88.
Wang K, Li M, Hakonarson H. ANNOVAR: functional annotation of genetic variants from high-throughput sequencing data. Nucleic Acids Res 2010; 38: e164.
Wang Y, Zhang H, Ling F. Coexistence of a single cerebral arteriovenous malformation and spinal arteriovenous malformation. Neurol India 2009; 57: 785–8.

Downloaded from https://academic.oup.com/brain/article/142/1/23/5240918 by guest on 21 August 2022